Electrical Behaviour and Microstructural Characterization of Magnesia Co-doped ScSZ Nanopowders Synthesized by Urea Co-precipitation

Grazia Accardo[*,a], Gianfranco Dell'Agli[b], Domenico Frattini[a], Luca Spiridigliozzi[b], Suk Woo Nam[a] , Sung Pil Yoon[a]

[a] Fuel Cell Research Center, KIST-Korea Institute of Science and Technology, Hwarang-ro 14-gil 5, Seongbuk-gu 136-791, Seoul, South Korea
[b] Department of Civil and Mechanical Engineering and INSTM Research Unit, University of Cassino and Southern Lazio, Via G. Di Biasio 43, 03043, Cassino (FR), Italy
d16605@kist.re.kr

In this study Scandia-doped zirconia co-doped with MgO, $(MgO)_{0.03}(ZrO_2)_{0.88}(Sc_2O_3)_{0.09}$, was synthetized by using the urea co-precipitation method in hot aqueous solution. MgO was added to prevent the transformation of cubic fluorite Sc-doped ZrO_2 into rhombohedral phase, with worst electrical properties. The as-prepared powders were completely amorphous and, by a calcination step at 500 °C for 1 h, full conversion to fluorite phase occurred preserving the nano size character of powders. The presence of MgO allowed to effectively stabilize the cubic fluorite phase also after a prolonged thermal treatment at 1200 °C. The nanometric feature of the powder aided the sintering step of this material at 1600 °C. The EIS electrical characterization revealed that its ionic conductivity is $7.3 \cdot 10^{-2}$ S/cm and $2.8 \cdot 10^{-2}$ S/cm at 800 °C and 700 °C, respectively. Therefore, this material is suitable as ceramic electrolyte in SOFC operated at intermediate temperatures.

1. Introduction

In the last 5 years one of the main trends in the renewable energy field was the development of high temperature fuel cell systems for stationary power generation. These systems are represented by Molten Carbonate Fuel Cells (MCFCs) and Solid Oxide Fuel Cells (SOFCs) integrated with reforming units, turbines or post-combustion regenerators (Jienkulsawad et al., 2015; Simasatitkul et al., 2015). In order to reduce carbon emissions, fossil fuels consumption and electric power fluctuation, these devices can be coupled to photovoltaic and wind energy to realize hybrid polygeneration systems for industrial and residential applications (Lin et al., 2015). The distinctive features of these innovative designs are an electric efficiency and operational flexibility higher than traditional electric power plant together with a reduction of capital costs and of CO_2 emissions (Lin et al., 2015; Tippawan et al., 2015). In particular, an engineered microstructure of components for SOFCs can increase performance and transport properties to enhance electrochemical reactions throughout the cell (Bertei et al., 2013). This is due to the fact that SOFCs, with proper electrolytes, can be operated at lower temperatures, i.e. 600-800 °C, thus opening the window of the so-called Intermediate Temperature SOFCs (ITSOFCs) which have a higher operability and lifetime thanks to the chemical stability and high ionic conductivity of ceramic electrolytes, different from standard Yttria-Stabilized Zirconia (YSZ). Ceramic electrolytes of SOFCs represent the core component of the electrochemical ion transport inside the cell. They are a robust and solid separation membrane which conduct charged ions from cathode to anode through a series of hops inside reticular vacancies. The hopping mechanism is allowed by large interionic open spaces due to oxygen vacancy defects in fluorite-like lattices (Mahato et al., 2015). Therefore, the most important oxide systems are considered to be CeO_2 and ZrO_2 for their fluorite lattice. Moreover, in order to introduce oxygen vacancies to facilitate the ionic transport, these systems can be easily doped and co-doped with other metal cations to obtain ternary and quaternary systems, respectively, with more oxygen vacancies (Jiang and Hertz, 2014).

An interesting route for improving the total ionic conductivity of solid oxide electrolytes is co-doping these materials with Bi, Cu, Mg, Fe, Li (Accardo et al., 2016b). Traditional routes are based on solid solution mixtures where the as-prepared electrolyte powders are added to co-doping metal oxides powders via mechanochemical mixing. The final powders require the use of a densifier for sintering, which can influence the purity of final electrolyte and the electrochemical properties. Several electrolytes, based on ZrO_2 and CeO_2 and different synthesis routes, have been studied by doping CeO_2 with lanthanides and ZrO_2 with transition and alkaline metals (Dell'Agli et al., 2016; Accardo et al., 2016a). In the case of ZrO_2, an activation energy >1 eV was observed and total ionic conductivity increases with dopant concentration until the complete stabilization of the fluorite structure is achieved and conductivity reaches its maximum (σ= 0.28-0.34 S/cm at 1000 ˚C, Badwal et al., 2000) and then decreases due to dopants solubility limits. In literature, these limits were found to be 9-11 % for $(Sc_2O_3)_x$–$(ZrO_2)_{1-x}$ systems (Gomez and Hotza, 2016) and 8-11 % for $(Y_2O_3)_x$–$(ZrO_2)_{1-x}$ systems (Liu et al., 2015). ScSZ co-doped with MgO has been studied recently as possible ceramic electrolyte for ITSOFC (Sonoyama et al., 2015; Kumar et al., 2016) and the positive effect of MgO, in stabilizing the cubic scandia-doped zirconia, needs more work to be confirmed.

The aim of this work is to investigate the electrical and microstructural properties of ScSZ nanopowders co-doped with magnesia, prepared via the Urea-Based Homogeneous co-Precipitation (UBHP) route. This synthesis procedure was chosen because, as reported in a previous work (Accardo et al., 2017), it is an emerging method to synthesize co-doped oxides with very interesting properties for SOFC applications. UBHP is simpler and less expensive with respect to other routes proposed. The thermal behavior of as-prepared and calcined powders was evaluated by simultaneous differential scanning calorimetry and thermogravimetric analysis (TGA-DSC) and crystallite size was determined by X-ray diffraction analysis (XRD). No sintering densifiers, dispersant or protective agent were used during sintering. The microstructure was examined by scanning electron microscopy (SEM) and transmission electron microscopy (TEM), the ionic conductivity was measured by electrochemical impedance spectroscopy (EIS).

2. Materials and Methods

2.1 Synthesis procedure

Zirconium oxychloride octahydrate ($ZrOCl_2 \cdot 8H_2O$, 99.9 %), Sc_2O_3 (99.9 %), $Mg(NO_3)_2 \cdot 6H_2O$ (99 %) and urea ($CO(NH_2)_2$ 99+ %) are used as starting materials. Sc_2O_3 was dissolved in HNO_3 5 M with a concentration 4 g/L. The solution of the precursors was prepared using the proper amount of $ZrOCl_2 \cdot 8H_2O$, $Mg(NO_3)_2.6H_2O$, urea and solution of Sc_2O_3 in order to obtain the following composition: $(ZrO_2)_{0.88}(Sc_2O_3)_{0.09}(MgO)_{0.03}$ ($Mg_{0.028}Sc_{0.165}Zr_{0.807}O_{2-x}$), referred as Sc9Mg3ZrO2 in the following. The total cations concentration in the solution of the precursor was fixed at 0.1 M whereas the urea concentration was 2.5 M. The co-precipitation of hydrous Sc9Mg3ZrO2 was caused by the thermal decomposition of urea (in ammonia and carbon dioxide) occurring at temperature >83 °C. As a result of the slow decomposition of urea, a slow and homogeneous rising of the pH of the solution takes place, leading to the precipitation of hydrous oxide particles avoiding the localized distribution of the reactants. The formed co-precipitate is aged in boiling conditions under vigorous stirring for 1 h. During the last two steps a total reflux apparatus is used to avoid the escape of the evaporated solution to maintain constant conditions. The co-precipitate was filtered and washed repeatedly with deionized water in order to remove the undesired ions, after drying at 60 °C overnight and then a calcination step was carried out in air at 500 °C for 1 h. The powders were finally grinded and compacted in cylindrical pellets by uniaxial pressing. Sintering was performed in air at 1600 °C with a dwell time of 3 h. The relative density of sintered pellets was determined by hydrostatic balance according to the Archimedes' method.

2.2 Characterization of powders and compacts

The present phases of both as-prepared and calcined powders were evaluated by XRD using a Panalytical X'PERT MPD diffractometer. The primary particles size, d, was calculated by the Scherrer formula (using X'Pert High Score Panalytical software) from the peak profile with a pseudo-Voigt function as peak modelling:

$$d = \frac{K\lambda}{B\,cos\theta} \tag{1}$$

where K is the shape factor (assumed equal to 0.89), λ the X-ray wavelength (0.1541 nm for Cu Kα1), θ the Bragg's angle of the most intense diffraction peak and B the full width at half maximum of the same peak, corrected for the instrumental broadening, given by:

$$B = B_{sample} - B_{instr} \tag{2}$$

where B_{instr} was determined using standard polycrystalline silicon. The thermal behaviour of Sc9Mg3ZrO2 powders was evaluated by TGA-DSC (Thermoanalyzer STA 409, Netzsch) in air at a heating rate of 10 °C/min

up to 1200 °C using αAl_2O_3 as reference. Morphology and particle size were analysed by TEM (Tecnai F20 G^2, FEI Co.) while the microstructure of pellets, sintered at 1600 °C for 3 h, was observed by SEM (Inspect F, FEI Co.). EIS measurements were performed on pellets by painting a Platinum conductive paste on both sides and then treating at 700 °C for 1 h to ensure good adhesion and proper electric contact. Measurements were carried out in the 300-800 °C temperature range using a frequency response analyzer (FRA, Solartron 1260), coupled with a dielectric interface (Solartron 1296) in a frequency range between 0.01 Hz and 5 MHz with an AC voltage amplitude of 50 mV. The data analysis of impedance plots was carried out by ZsimpWin software.

3. Results and Discussion

The TGA-DSC thermal behaviour of the co-precipitate is reported in Figure 1. This product is very similar to that of analogous zirconia-based materials prepared by coprecipitation (Dell'Agli et al., 2005; Dell'Agli et al., 2008). The first thermal event is represented by a very broad endothermic peak in the temperature range 100-300 °C and related to the evolution of the water vapour.
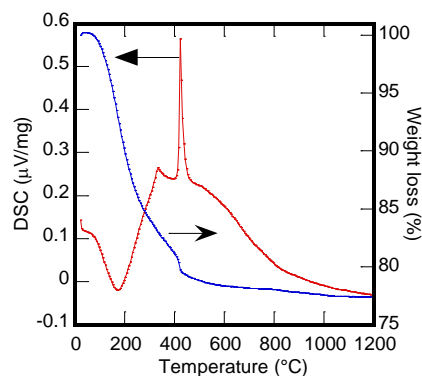

Figure 1: TGA-DSC thermograph of as-synthesized powders.

From the TG thermograph a total weight loss equal to 22.6 % results, which agrees perfectly with the theoretical value, i.e. 22.5 %, deriving from the thermal decomposition of the mixed hydroxides corresponding to the anhydrous final nominal composition ($Mg_{0.028}Sc_{0.165}Zr_{0.807}O_{2-x}$). Furthermore, a very sharp exothermic peak is present at 422 °C representing the conversion of amorphous phase to cubic fluorite structure.

Therefore, a calcination step at 500 °C for 1 h and a long-term calcination at 1200 °C for 48 h were carried out and the relative diffraction pattern recorded to show the evolution and stability of the crystalline structure. The XRD spectra are shown in Figure 2.
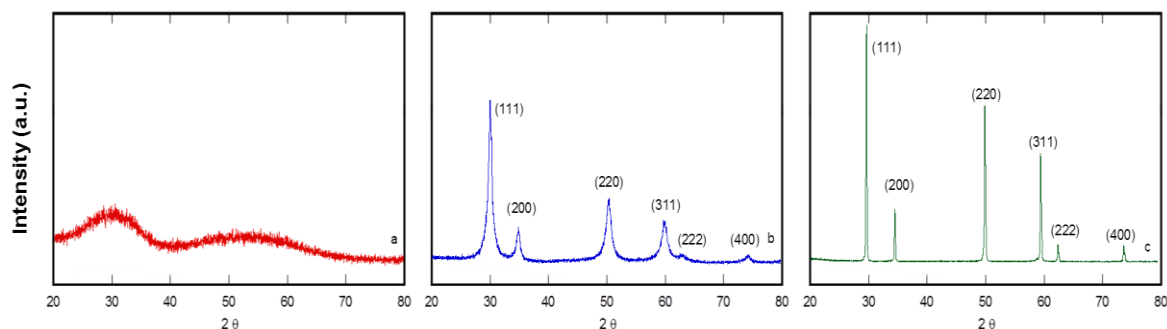

Figure 2: XRD of powders as-prepared (a), calcined at 500 °C for 1 h (b), and calcined at 1200 °C for 48 h (c).

From the urea-based co-precipitation, an amorphous hydrous doped-zirconia xerogel is firstly obtained (Figure 2a). After calcination, Figure 1b confirms the crystallization of fluorite cubic phase of co-doped zirconia, as all the XRD peaks are attributable to it. However, Sc-doped zirconia fluorite cubic phase can turn into a rhombohedral phase at about 600 °C. In order to prove the actual stabilization of the fluorite cubic phase, the XRD pattern after a prolonged thermal treatment at 1200 °C for 48 h, is shown in Figure 2c. Only the XRD peaks of the cubic fluorite phase are present so the powders are stabilized in the fluorite phase. In addition, a shift towards higher 2θ of the Bragg angles, with respect to the cubic pure zirconia, due to the formation of the substitutional solid solution and very sharp peaks are visible as a result of the remarkable grain growth due to the very long thermal treatment. Calcined powders have a regular spherical morphology, as it can be seen in the TEM micrographs before and after calcination (Figure 3). The as-prepared xerogel is amorphous but after calcination at 500 °C, agglomerates of nanoparticles, whose size is about 10 nm, appear clearly.
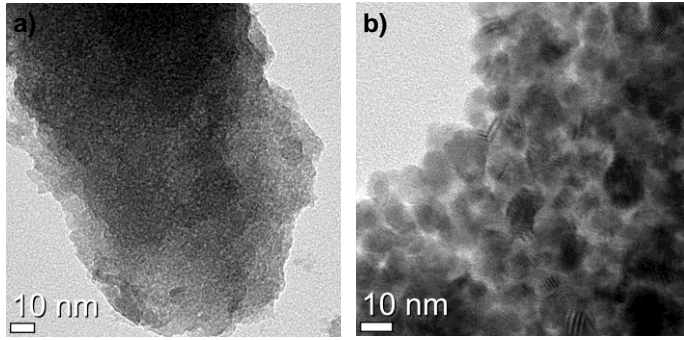
Figure 3: TEM micrographs of Sc9Mg3ZrO2 powders: (a) as-prepared; (b) after calcination.

The determination of lattice parameter, by a least square procedure (Suryanarayana and Norton, 1998), provides as result a = 0.5096 nm which is in very good agreement with 0.5088 nm, i.e. the literature data (Sonoyama et al., 2015) reported for the cubic zirconia with the same composition. The particle size of calcined powders, determined by the Scherrer formula, is 13.6 nm thus confirming the nano size feature of powders observed by TEM. These powders were uniaxially compacted and finally sintered at 1600 °C for 3 h. The relative microstructure was analysed by SEM and an exemplary micrograph is reported in Figure 4.
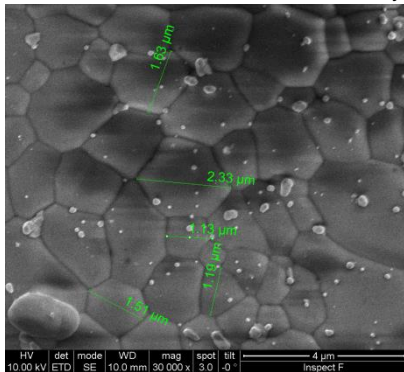

Figure 4: Microstructure of Sc9Mg3ZrO2 pellet at 30,000 X.

The sintered pellet appears well densified and a relative density of about 97% was measured by hydrostatic balance. It can be observed the low amount of porosity, especially located at the grain boundary. Furthermore, the texture is characterized by prevailing equiaxed grains whose size is on the order of 1-2 μm.

This specimen was used for the electrochemical characterization by EIS and the impedance Nyquist plots for different temperatures are reported in Figure 5.
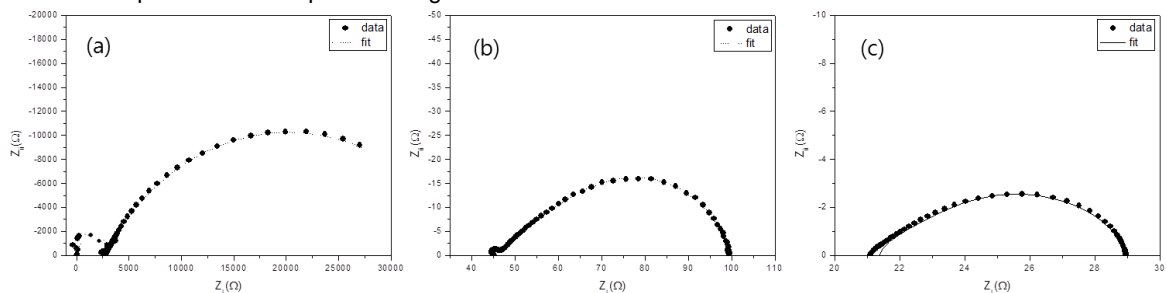

Figure 5: Nyquist plot of Sc9Mg3ZrO2 as function of temperature: (a) 300 °C; (b) 600 °C; (c) 650°C.

The impedance behaviour of polycrystalline electrolytes can be ascribed to three contributions: the grain interior (bulk), grain boundary conduction and electrode reaction, with characteristic frequencies increasing from the right to the left in the Nyquist plot. These contributions change with the operative temperature. The measured impedance spectra are typical for polycrystalline electrolytes with ionic current partially blocked by grain boundaries. In fact, the impedance spectrum of Sc9Mg3ZrO2 (Figure 5a), recorded at 300 ˚C, exhibit a distinct semi-circle at high frequencies and a second very large arc, observed at lower frequencies. According to the brick layer model the arcs related to grain boundary and bulk are observable only at low temperature. Therefore, the high frequency semi-circle at 300 ˚C is assigned to the bulk impedance, based on the capacitance value of 6.7 10^{-11} F. On the other hand, the value of 5.3 10^{-9} F reflects the effect of grain

boundary in the low frequency region. The grain boundary arc is always visible between 300 °C-600 °C but it tends to disappear (Figure 5b). Above 600 °C, only the contribution related to the electrode reaction influences the total ionic conductivity, as showed in Figure 5c. This is due to a change in the conduction behaviour of grain boundary in the electrolyte. To better show this effect, the Arrhenius plot of grain boundary conductivity and total ionic conductivity are presented in Figure 6.
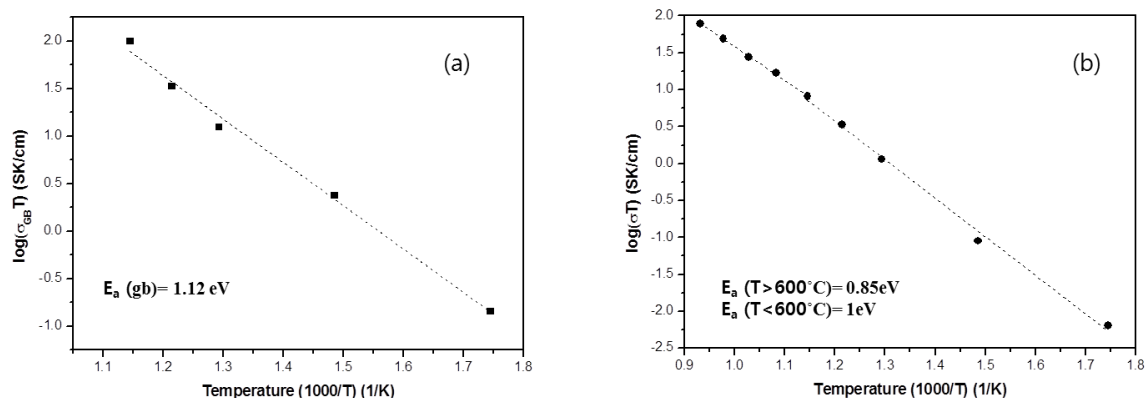

Figure 6: Arrhenius plot of (a) grain boundary conductivity, (b) total ionic conductivity.

The experimental data have not a perfect linear dependence with temperature, because the conduction mechanism changes at a transition temperature of 600 °C related to the grain boundary contribution. As a consequence, the slope of the Arrhenius changes and two distinct values, i.e. activation energies, can be retrieved from data fitting. The grain boundary conductivity recorded in the temperature range 300-600 °C is one order of magnitude higher than the total ionic conductivity as confirmed by the space charge layer (SCL) theory. This theory states that when structural defects are concentrated in a narrow region of the grain boundary, an energy limit, the so-called Schottky barrier height (Souza, 2013), is present and an additional amount of energy is required to ionic species to overcome this barrier. As showed in the Arrhenius plot of total ionic conductivity, Sc9Mg3ZrO2 has a high conductivity ($7.3 \cdot 10^{-2}$ -$1.0 \cdot 10^{-2}$ S/cm) in the operative temperature of IT-SOFC (800-600 °C) compared with literature. In fact, the maximum value recorded at 800 °C for a ceria-based electrolyte is $7 \cdot 10^{-2}$ S/cm, higher than traditional zirconia-based electrolyte ($3 \cdot 10^{-2}$ S/cm) (Mahato et al., 2015). For a scandia–yttria–zirconia system, it was found ionic conductivities in the range of $1.4 \cdot 10^{-2}$ -$5.18 \cdot 10^{-2}$ S/cm at 800 °C (Politova and Irvine, 2004). Other authors reported a value of $2 \cdot 10^{-2}$ S/cm at 800 °C after long sintering cycle (Sonoyama et al., 2015).

4. Conclusions

With the UBHP it was possible to synthesize Mg-Sc co-doped zirconia with nominal composition $Mg_{0.028}Sc_{0.165}Zr_{0.807}O_{2-x}$. The as-synthesized sample is amorphous but with a calcination step at 500 °C it crystallizes in the desired fluorite structure. The added MgO favours the real stabilization of this phase and in fact also after a prolonged thermal treatment at 1200 °C no decomposition appears. The nanometric characteristics of the powders favour the sintering and a well densified pellets is obtained after firing at 1600 °C for 3 h. The electrical behaviour is of great interest as the synthesis method and the Mg co-doping showed to increase the conductivity of zirconia-based electrolytes for IT-SOFC application, compared to the common ceria-based electrolytes. This is due to the enhanced powder morphology and hence the resulting microstructure after sintering. In conclusion, the synthesis route proposed together with the Mg co-doping is encouraging alternative methods to obtain high performance zirconia-based electrolytes for IT-SOFCs.

References

Accardo G., Ferone C., Cioffi R., Frattini F., Spiridigliozzi L., Dell'Agli G., 2016a, Electrical and microstructural characterization of ceramic gadolinium-doped ceria electrolytes for ITSOFCs by sol-gel route. Journal of Applied Biomaterial and Functional Material, 14, 35-41, DOI: 10.5301/jabfm.5000265.

Accardo G., Ferone C., Cioffi R., 2016b, Influence of lithium on the sintering behavior and electrical properties of Ce0.8Gd0.2O1.9 for Intermediate-Temperature Solid Oxide Fuel Cells. Energy Technology, 4, 409-416, DOI: 10.1002/ente.201500275.

Accardo G., Spiridigliozzi L., Cioffi R., Ferone C., Di Bartolomeo E., Yoon S.P., Dell'Agli G., 2017, Gadolinium doped ceria nanopowders synthetized by Urea-based Homogenous-Precipitaion (UBHP). Materials Chemistry and Physics, DOI: 10.1016/j.matchemphys.2016.11.060.

Badwal S.P.S., Ciacchi F. T., Milosevic D., 2000, Scandia–zirconia electrolytes for intermediate temperature solid oxide fuel cell operation. Solid State Ionics, 136, 91-99, DOI: 10.1016/S0167-2738(00)00356-8.

Bertei A., Nucci B., Nicolella C., 2013, Engineered electrode microstructure for optimization of solid oxide fuel cells. Chemical Engineering Transactions, 32, 2293-2298, DOI: 10.3303/CET1332383.

Dell'Agli G., Spiridigliozzi L., Marocco A., Accardo G., Ferone C., Cioffi R., 2016, Effect of the mineralizer solution in the hydrothermal synthesis of gadolinium-doped (10% mol Gd) ceria nanopowders. Journal of Applied Biomaterial and Functional Material, 14, 189-196, DOI: 10.5301/jabfm.5000282.

Dell'Agli G., Mascolo G., Mascolo M.C., Pagliuca C., 2005, Crystallization-stabilization mechanism of yttria-doped zirconia by hydrothermal treatment of mechanical mixtures of zirconia xerogel and crystalline yttria. Journal of Crystal Growth, 280/1-2, 255-265, DOI: 10.1016/j.jcrysgro.2005.03.004.

Dell'Agli G., Mascolo G., Mascolo M.C., Pagliuca C., 2008, Drying effect on thermal behaviour and structural modification of hydrous zirconia gel. Journal of the American Ceramic Society, 91, 3375-3379, DOI: 10.1111/j.1551-2916.2008.02635.x

Gomez S.Y. and Hotza D., 2016, Current developments in reversible solid oxide fuel cells. Renewable and Sustainable Energy Reviews, 61, 155-174, DOI: 10.1016/j.rser.2016.03.005

Jiang J. and Hertz J.L., 2014, On the variability of reported ionic conductivity in nanoscale YSZ thin films. Journal of Electroceramics, 32, 37-46, DOI: 10.1007/s10832-013-9857-1.

Jienkulsawad P., Saebea D., Patcharavorachot Y., Arpornwichanop A., 2015, Design of the integrated solid oxide fuel cell and molten carbonate fuel cell system to reduce carbon dioxide emissions. Chemical Engineering Transactions, 43, 2191-2196, DOI: 10.3303/CET1543366.

Kumar A., Jaiswel A., Sanbui M., Omar S., Scandia stabilized zirconia-ceria solid electrolyte (xSc1CeSZ, 5<x<11) for IT-SOFCs: Structure and conductivity studies. 2016, Scripta Materialia, 121, 10–13, DOI: 10.1016/j.scriptamat.2016.04.023.

Lin M.-H., Adi V.S.K., Chang C.-T., 2015, Flexible photovoltaics/fuel cell/wind turbine (pvfcwt) hybrid power system designs. Chemical Engineering Transactions, 45, 559-564, DOI:10.3303/CET1545094.

Liu T., Zhang X., Yuan L., Yu J., 2015, A review of high-temperature electrochemical sensors based on stabilized zirconia. Solid State Ionics, 283, 91-102, DOI: 10.1016/j.ssi.2015.10.012.

Mahato N., Banerjee A., Gupta A., Omar S., Balani K., 2015, Progress in material selection for solid oxide fuel cell technology: A review. Progress in Material Science, 72, 141-337, DOI: 10.1016/j.pmatsci.2015.01.001.

Politova T.I. and Irvine J.T.S., 2004, Investigation of scandia–yttria–zirconia system as an electrolyte material for intermediate temperature fuel cells—influence of yttria content in system $(Y_2O_3)_x(Sc_2O_3)_{(11-x)}(ZrO_2)_{89}$. Solid State Ionics, 168, 153-165, DOI:10.1016/j.ssi.2004.02.007.

Simasatitkul L., Mahisanan C., Arpornwichanop A., 2015, Performance analysis of the solid oxide fuel cell and oxyfuel combustion integrated system with different recycling methods. Chemical Engineering Transactions, 45, 1045-1050, DOI:10.3303/CET1545175.

Sonoyama N., Garcia Martin S., Amador U., Imanishi N., Ikeda M., Erfu N., Tanimura H., Hirano A., Takeda Y., Yamamoto O., 2015, Crystal structure and electrical properties of Magnesia co-doped Scandia Stabilized Zirconia. Journal of The Electrochemical Society, 162, F1397-F1401, DOI: 10.1149/2.0231514jes

Souza E.C.C., 2013, Electrochemical properties of doped ceria electrolyte under reducing atmosphere: bulk and grain boundary. Journal of electroceramics, 31, 245-253, DOI:10.1007/S10832-013-9826-8.

Suryanarayana C., Norton M.G., Eds., 1998, X-Ray Diffraction A Practical Approach, Springer, Berlin, Germany.

Tippawan P., Arpornwichanop A., Dincer I., 2015, Exergoenvironmental analysis of heat recovery from solid oxide fuel cell system for cooling applications. Chemical Engineering Transactions, 43, 2203-2208, DOI: 10.3303/CET1543368.